King's Research Portal

Accepted Manuscript

Automated quantification of mitral valve geometry on multi-slice computed tomography in patients with dilated cardiomyopathy – Implications for transcatheter mitral valve replacement

Tom Banks, Orod Razeghi, Ioannis Ntalas, Waqar Aziz, Jonathan M. Behar, Rebecca Preston, Brian Campbell, Simon Redwood, Bernard Prendergast, Steven Niederer, Ronak Rajani

Automated Quantification of Mitral Valve Geometry on Multi-Slice Computed Tomography in Patients with Dilated Cardiomyopathy – Implications for Transcatheter Mitral Valve Replacement

Tom Banks *, Orod Razeghi PhD **, Ioannis Ntalas MD PhD *, Waqar Aziz MBBS MRCP *, Jonathan M. Behar MBBS MRCP *, Rebecca Preston FRCR ***, Brian Campbell PhD *, Simon Redwood MD FRCP FACC *, Bernard Prendergast PhD FRCP FESC *, Steven Niederer PhD **, Ronak Rajani MD FRCP FESC FSCCT *, **

* Department of Cardiology, Guy's and St Thomas' NHS Foundation Trust, London. United Kingdom.

** Division of Imaging Sciences and Bioengineering, King's College London, London. United Kingdom.

*** Department of Radiology, Guy's and St Thomas' NHS Foundation Trust, London. United Kingdom.

Address for correspondence

Tom Banks, Cardiac Outpatients, North Wing, St Thomas' Hospital, Westminster Bridge Road, London, SE1 7EH. United Kingdom.

Tel: +44 7837 806 459

Email: Tom.Banks@gmail.com

Abstract

Objectives

The primary aim of this study was to quantify the dimensions and geometry of the mitral valve complex in patients with dilated cardiomyopathy and significant mitral regurgitation. The secondary aim was to evaluate the validity of an automated segmentation algorithm for assessment of the mitral valve compared to manual assessment on computed tomography.

Background

Transcatheter mitral valve replacement (TMVR) is an evolving technique which relies heavily on the lengthy evaluation of cardiac computed tomography (CT) datasets. Limited data is available on the dimensions and geometry of the mitral valve in pathological states throughout the cardiac cycle, which may have implications for TMVR device design, screening of suitable candidates and annular sizing prior to TMVR.

Methods

A retrospective study of 15 of patients with dilated cardiomyopathy who had undergone full multiphase ECG gated cardiac CT. A comprehensive evaluation of mitral valve geometry was performed at 10 phases of the cardiac cycle using the recommended D-shaped mitral valve annulus (MA) segmentation model using manual and automated CT interpretation platforms. Mitral annular dimensions and geometries were compared between manual and automated methods.

Results

Mitral valve dimensions in patients with dilated cardiomyopathy were similar to previously reported values (MA_{area} Diastole: 12.22 ± 1.90 cm^2), with dynamic changes in size and geometry between systole and diastole of up to 5%. The distance from the centre of the MA to the left ventricular apex demonstrated moderate agreement between automated and manual methods ($\rho_c = 0.90$) with other measurements demonstrating poor agreement between the two methods ($\rho_c = 0.75 - 0.86$).

Conclusions

3

Variability of mitral valve annulus measurements are small during the cardiac cycle. Novel automated algorithms to determine cardiac cycle variations in mitral valve geometry may offer improved segmentation accuracy as well as improved CT interpretation times.

Key words: Mitral valve; Geometry; Computed Tomography, Transcatheter mitral valve replacement.

Condensed Abstract

Transcatheter mitral valve replacement is an evolving technique which relies heavily on the lengthy evaluation of cardiac computed tomography datasets. Data regarding the dimensions and geometry of the mitral valve in pathological states is limited. This may in turn have implications for transcatheter mitral valve replacement device design, screening of suitable candidates and annular sizing. Our study firstly demonstrates that in patients with dilated cardiomyopathy, changes in the mitral valve annulus areas are small. Secondly, we show the potential clinical utility of automated techniques to evaluate the mitral valve complex.

Abbreviations list

MR	Mitral regurgitation
CT	Computed tomography
ECG	Electrocardiogram
LCCC	Lin's concordance correlation coefficient
TAVR	Transcatheter aortic valve replacement
TMVR	Transcatheter mitral valve replacement

Introduction

The recommended treatment strategy for patients with severe symptomatic mitral regurgitation (MR) is surgical mitral valve repair or replacement. However, a large proportion of patients suffering from MR are unsuitable for surgery owing to co-existing morbidities (1). Following the success of transcatheter aortic valve replacement (TAVR) (2), there has been similar interest in the development of transcatheter mitral valve replacement (TMVR). Before this approach can achieve a similar acceptance to TAVR it will need to demonstrate similar efficacy outcomes and be proven to be a viable option to bridge this therapeutic gap (3,4). This will require optimal patient selection and procedure planning to account for the more complex anatomy of the mitral valve and its apparatus.

Although early studies have defined the 3-dimensional (3D) geometry of the mitral valve and its dynamic changes throughout the cardiac cycle in healthy individuals (12,13), limited data are available in pathological states (14), especially in patients with MR (13). Patients with dilated cardiomyopathy represent a distinct subgroup where dilation of the left ventricle, increased wall stress and systolic dysfunction result in papillary muscle displacement, chordae tendinae traction, mitral valve leaflet tenting and mitral annulus dilatation. One result of these changes is the development of functional mitral regurgitation (12,14). Furthermore, existing studies are limited by their methodological heterogeneity and applicability to the requirements of TMVR. These namely being: small sample sizes (14,15); failure to quantify the mitral valve throughout the full cardiac cycle (11,14); and differences in segmentation models (5). It has therefore become important to establish a standardised approach to the assessment of the mitral valve to ensure optimal TMVR device design and patient outcomes (16).

The large reliance on pre-procedural imaging with numerous measurements requires cumbersome and time–consuming processing of large datasets and expert interpretation (15,17). An automated system may streamline pre-procedural workups as seen with similar semi-automated algorithms applied to other cardiac structures acquired with computed tomography (CT) (11,17).

The aims of the current study were 1) to define the dynamic changes in mitral valve geometry throughout the cardiac cycle in patients with dilated cardiomyopathy and 2)

to explore the accuracy of a novel automated tracking algorithm for valve segmentation.

Methodology

Study cohort

This study involved the retrospective evaluation of 17 consecutive patients with dilated cardiomyopathy with permanent pacemakers in situ who were scheduled to have pacemaker upgrades to cardiac resynchronisation therapy. Helical scans with retrospectively ECG-gated image reconstruction were performed in these patients as part of a previous study protocol to evaluate CT dyssynchrony, coronary venous anatomy and delayed enhancement by CT. All patients were >18 years of age and had no contraindication to cardiac CT. No patient in this the study had undergone prior aortic and/or MV repair/replacement that may have introduced MV apparatus distortion to the planned measurements (20).

All data sets were evaluated manually at all stages of the cardiac cycle and thereafter automatically using a locally developed mitral valve tracking computer algorithm. Written informed consent was obtained from all patients for the original study, while the local research and governance board further approved the use of the acquired data for the purposes of mitral valve geometry evaluation.

Cardiac CT acquisition

All cardiac CT scans were performed using a Philips Brilliance iCT 256-slice MDCT scanner (Philips Healthcare, Best, The Netherlands). Intravenous metoprolol was used to achieve a heart rate of < 65 beats/min (<100 beats per minute for those in atrial fibrillation). A total of 100 mls of intravenous contrast (Omnipaque, GE Healthcare, Princeton, NJ, USA) was injected (5 mL/s) via a power injector into the antecubital vein. Ascending aorta contrast triggered, helical scanning was performed with a single breath-hold technique after a 10-12 second delay. The scanning parameters included a heart rate dependent pitch of 0.2-0.45, a gantry rotation time of 270 ms, a tube voltage of 100 or 120 kVp depending on the patient's body mass

index and a tube current of 125-300mA, depending upon the thoracic circumference. Retrospectively ECG-gated image reconstruction was used to generate 10 data sets per cardiac cycle.

CT Data analysis

Assessment of the mitral valve dimensions was performed in two separate platforms for manual and automatic methods, with both allowing double-oblique multiplanar reformatted reconstructions of the heart (21). Manual assessment of the mitral apparatus was performed in OsiriX (Pixmeo SARL, Bernex, Switzerland), while automatic tracking was performed in a dedicated platform developed in MatLab (MathWorks, Natick, MA, USA).

Pre-processing of CT datasets was required for the automatic tracking algorithm including cropping of CT images to include only the heart structures, allowing for reduced image processing times.

Mitral Valve Anatomy – determination of optimal measuring planes

The mitral annulus is a fibro-muscular junction dividing the left atrium and the left ventricle. Its complex 3D saddle shaped structure is defined by the anterior and posterior horn and inferiorly positioned anterolateral and posteromedial commissures (3,10,12) (Fig 1). The fibrous region of the annulus is located at the aorto-mitral continuity, between the medial and lateral trigones. The predominantly muscular posterior border predisposes the structure to remodeling unlike its fibrous anterior counterpart (6). The anterior and posterior mitral leaflet are supported by further sub-valvular structures. All of which play an important role in the function of the mitral valve in healthy and pathological states (12).

Segmentation models

A plethora of 2D and 3D segmentation models are apparent in the assessment of the mitral valve. The D-shaped, non-planar model and protocol for mitral annulus

assessment has recently been proposed and supported as an applicable and valid model in the context of TMVR (5, 21).

Mitral valve evaluation

Manual quantification

Prior to assessment of the mitral valve, each CT data set was aligned into 4 chamber, 2 chamber and short axis views at the level of the mitral annulus (3,5,21). The measurements taken are described in Table 1 and illustrated in Figure 2. All of the 10 measurements were performed at phase 0% of the cardiac cycle and then repeated through all of the remaining phases to give a total number of measurements for one scan of 100. The average time taken for the complete evaluation of one entire CT data set was approximately 60 minutes across all 10 phases. All manual evaluation was performed by a SCCT Level III verified expert in cardiac CT with 8 years' experience (RR).

Automatic quantification

For automatic quantification, each data set required initial segmentation in one phase (0%) (Table 1). The locally developed tracking algorithm then performed automated measurements of all parameters in the remaining 9 phases. All measurements were performed offline by an individual trained in cardiac CT (TB) by batch analysis and then confirmed by an independent SCCT verified Level III expert in cardiac CT (RR).

Statistical analysis

For the manual measurements across systole and diastole, means ± SD, median, the 1st and 3rd interquartile and percentage change were calculated and expressed in graphical format. All continuous variables were expressed as means ± SD. Paired sample t-tests were then performed across all 10 parameters to compare manual and automatic measurements for the initial phase (0%) used to segment and

quantify the mitral valve complex. Bonferroni correction was applied to adjust for multiple comparisons using the following formula:

$$\propto = \frac{0.05}{n}$$

Where n = 10 (number of comparisons), producing a *p* <0.005 as the accepted level of significance.

To assess the agreement of the automated tracking algorithm with manual measurements, Lin's concordance correlation coefficient (LCCC) was applied to all 10 measurements in the short and long-axis views. The following guidelines were used to assess the strength of agreement (23): Almost perfect (ρ_c >0.99), Substantial (ρ_c = 0.95 – 0.99), Moderate (ρ_c = 0.90 – 0.95), Poor (ρ_c <0.90).

Results

From the initial 17 patients, only 15 datasets were used in the final analysis. One dataset was excluded owing to incomplete data and 1 case owing to suboptimal image quality. A total of 35 phases of 340 were excluded in the mitral valve quantification due to variable slice thickness on multiplanar reformatted reconstructions and subsequent image distortion. The baseline characteristics for the study population are given in table 2.

The Mitral Annulus.

The mean values (± SD) with lower and upper quartiles measured at the level of the MA, sub and supra apparatus are displayed in table 3. The intercommissural diameter was greater than that of the anterior – posterior horn diameter in both systole and diastole, revealing a non-circular structure in the context of a D-shaped model, truncating the anterior peak of the annulus. The mean values for annulus area (diastolic: 12.2 cm^2 ± 1.9; systolic: 11.6 cm^2 ± 1.6), posterior perimeter (diastolic: 101 mm ± 8; systolic: 99 mm ± 7), trigone to trigone diameter (diastolic: 26 mm ± 2; systolic: 25 mm ± 2.8), intercommissural diameter (diastolic: 42 mm ± 3.3; systolic: 41mm ± 2.9) and anterior to posterior peak diameter (diastolic: 35 mm ± 3.4; systolic: 33 mm ± 3.1) were comparable in diastole and systole (Table 3). The

largest changes between systole and diastole were seen at the anterior to posterior peak (5.3% increase in diastole, p = 0.005), with a subsequent 5.5% increase in MA$_{area}$ (p = 0.045). There were no differences in the intercommissural diameter and trigone to trigone diameter were noted (0.8%, p = 0.58 and 3.3%, p = 0.14, respectively).

Across the retrospectively ECG gated cardiac CT scan, not all parameters for all patients were largest during diastole (phase 60%). The posterior perimeter of the annulus revealed larger dimensions at 50% whilst the trigone to trigone diameter and anterior to posterior diameter were both largest in phases 90% and 80%, respectively. Figure 3 illustrates the dynamic changes of the 5 short axis parameters across the full cardiac cycle (0% - 90%).

The left ventricle and left atrium.

The standard deviation between sub-valvular and supra-valvular dimensions was consistently >10%, demonstrating considerable inter-patient variability. Very small variations in LV, PM and LA dimensions between diastole and systole were noted (Table 3). The mean values of the LV long axis diameter showed no difference in the distance from the apex of the LV to the geometrical centre of the MV during systole (0.5%, LV$_{epi}$ p = 0.30, LV$_{endo}$ p = 0.71). The anterolateral papillary muscle was closer to the mitral valve geometrical centre compared to the posteromedial papillary muscle in both systole and diastole. There was no difference in the distance between the head of the posteromedial papillary muscle to the MV geometric centre during diastole (3.7%, p = 0.32). Conversely, smaller variations in the distance between the anterolateral PM and MV geometrical centre were noted (1.7%, p = 0.74), with the distance between the two larger during systole than diastole. Left atrial long axis diameter was similar in systole and diastole (58.5 mm vs. 57.7 mm, respectively) with a percentage change of 1.4% (p = 0.48).

Manual evaluation vs. automated evaluation.

There was no significant difference between initial manual and automated measurements at phase 0% except for two parameters; trigone to trigone diameter (manual measurement 26 mm $\pm$ 3 mm vs. automated measurement 28 $\pm$ 3mm; p < 0.005) and MA to anterolateral papillary muscle distance (manual measurement 31

mm $\pm$ 4 mm vs. automated measurement 27 $\pm$ 5mm; $p < 0.005$) (Table 4). Both parameters also revealed the lowest agreement on LCCC. The LCCC otherwise reported varying levels of agreement between manual and automated measures, with the MA to LV apical measures and LA diameter measures revealing moderate-poor agreement (Table 4). The MA to LV endocardial apex reported a moderate agreement ($\rho_c = 0.90$) between automated and manual measures. Figure 4 illustrates agreement across all parameters in correlation scatter plots.

Discussion

In the current study, we sought to systematically evaluate the deformation of the mitral valve complex throughout the cardiac cycle in patients with dilated cardiomyopathy, and to determine if automated evaluation of the MA was comparable to expert manual assessment. Our study confirms that MA_{area} and posterior perimeter are largest in early diastole and that there is little variability in apparatus dimensions across the cardiac cycle. Furthermore, we confirm that automated tracking may help to accelerate the evaluation of the complex MV anatomy and negate the need for arduous and time consuming manual assessment.

Our study confirms that mitral valve dimensions in dilated cardiomyopathy patients are larger in diastole (mean area: 12.2 cm^2 $\pm$ 1.9 cm^2) than those seen in previously studied healthy individuals (mean area: 8.3 cm^2 $\pm$ 2.3 cm^2) with considerable inter-patient variability noted across all dimensions (13). Additionally we confirm that the mitral valve annulus undergoes eccentric distortion during the cardiac cycle that results in an increased MA_{area} due to anterior-posterior horn dilatation as result of a pathophysiological process causing dilatation of the posterior muscular aspect of the annulus (11).

Whereas previous studies have revealed that MA_{area} is largest in mid systole (phase 30%), the present study revealed the smallest annular areas were noted in early systole (phase 0%-10%) and the largest areas occurred in early diastole (phase 60%). This likely reflects the unique annular dynamism seen in dilated cardiomyopathy patients as well as the nuances of the D-shaped segmentation model whereby due to truncation of the anterior horn of the annulus and its projected 2D area, coupled with the eccentricity of the distorted annular geometry, smaller annular areas are exhibited when compared to other segmentation techniques (15).

11

We observed that the mitral valve dimensions varied little during the cardiac cycle in patients with dilated cardiomyopathy. Compared to previous reported healthy individuals, the dynamic changes seen across the cardiac cycle were markedly suppressed in this cohort (15). Changes in MA_{area} of 5.5% between diastole and systole would appear to be largely attributed to changes in anterior to posterior horn diameter (5.3%), with very little changes in intercommissural diameter (0.8%). Furthermore, this study did not consider changes in the mitral valve annulus height, which has been observed to demonstrate a folding motion during systole contributing to larger changes in the MA_{area}. Previous studies have demonstrated impairment of this folding motion and changes in mitral valve annulus height in patients with mitral valve disease, concordant with the results noted in the current study (7). Although not fully understood, it has been suggested (15) that the deformed annular geometries and reduced dynamism found in functional may be due to impaired myocardial contraction and changes in left ventricular morphology associated with dilated cardiomyopathy. Indeed, the small changes seen in left ventricular long axis diameter between systole and diastole would support this notion, especially in impaired longitudinal contractility.

Left atrial enlargement is an independent predictor of annular dilatation (13). Our study revealed small changes in left atrial dimensions across systole and diastole, as well as left atrial dilatation seen in all patients. The mechanism of the left atrial and mitral valve interplay remains to be fully explored, but it is likely that left atrial dimensions have an important impact on mitral valve geometry. It is plausible that this is a result of direct morphological changes in the left atrium and therefore mitral valve dimensions, and/or a consequence of elevated left atrial pressures contributing to annular dilatation and the reduced annular dynamism similar to that as seen on the right side of the heart (24).

Implications for TMVR

Due to the early development state of TMVR, optimal device design yet has to be established. Indeed, early studies reveal encouraging early in-human experiences of a number of TMVR devices (1,25) but challenges remain, largely due to the complexity of the mitral valve and inappropriate device sizing. Concordant with previous research (11,16), our study has demonstrated broad variability between

patients, pathology and clinical status suggesting that the need for a tailored, patient specific approach to determining patient suitability and accurate device sizing. These unique insights into the dynamic geometry and dimension of the mitral valve using a D-shape segmentation model are more appropriate to the planar, tubular TMVR devices that are currently available and will enable better device development and design.

Mitral annulus geometry and dimensions are critical to prosthetic valve design and sizing for patients suitable for TMVR to minimise the likelihood of unfavorable outcomes associated with oversizing (left ventricular outflow tract obstruction obstruction, annular rupture) and under-sizing (prosthesis instability, paravalvular regurgitation) of valves. Although somewhat simplified at the aortic annulus with relatively stable geometry and reduced dynamism in calcified annuli (6,16), our study demonstrates that TMVR device sizing needs to accommodate changes in mitral valve geometry up to at least 5% throughout the cardiac cycle. In fact, previous studies have revealed changes as large as 12% (15). In particular, device sizing will need to accommodate larger changes in the anterior to posterior horn diameter to ensure optimal device functionality and therapeutic outcomes.

Left ventricular dimensions and dynamic changes will also have important implications on a number of factors, including procedural access (26), landing zone and device delivery (25). Despite revealing reduced dynamic changes in left ventricular geometry concordant with impaired systolic function seen in this dilated cardiomyopathy cohort, it may be prudent to consider the potential impact of successful therapeutic outcomes on left ventricular recovery. As demonstrated in severe organic mitral regurgitation (27) and aortic valve disease (28) improvements in left ventricular ejection fraction, longitudinal contractility, global strain and stroke volume may have important consequences on long-term changes in annular geometry and haemodynamics interacting with a TMVR prosthesis (29). Prosthetic valves sized and designed to accommodate a dilated, eccentric annular geometry may not be able to tolerate reciprocal recovery of annular dimensions and geometry following changes in left ventricular morphology and functional improvement.

Automated tracking algorithm

With the growing use of CT for transcatheter procedures to assess patient suitability and device sizing, manual assessment and interpretation of CT datasets is both time-consuming and cumbersome. Our study sought to evaluate the validity of an automated computational algorithm and compare its agreement with manual observer measurements of the MV complex.

Automation of large imaging datasets typical of magnetic resonance imaging and CT has been developed across medical disciplines to make analysis simpler and quicker. Studies have demonstrated faster acquisition, post-processing and interpretation of cardiac function, strain and volumes without the need for laborious manual analysis (30). Automated segmentation of valvular structures, in particular the aortic valve, has not only demonstrated analogous values with manual segmentation, but in fact revealed that automation allows for improved agreement of correct prosthesis sizing when compared to manual observers and greater standardisation of measurements with less intra-observer variability, particularly in less experienced observers (17).

Our study is the first to apply a novel automated algorithm to the mitral valve. Results demonstrate the validity of using an automated algorithm, indicating moderate agreement between manual and automated values for mitral annulus to left ventricular endocardial apex dimensions ($\rho_c = 0.90$), with many other measures showing poor agreement between the two methods ($\rho_c = 0.73$- 0.86). Indeed, our results demonstrate encouraging agreement between manual and automated methods particularly for posterior perimeter, MA_{area}, intercommissural diameter, mitral annulus to LV_{endo}/LV_{epi} and mitral annulus to left atrium superior wall, all of which had the highest agreement across all measures and no significant difference ($p<0.005$) between phase 0%.

Several factors may have contributed to the imperfect agreement between the manual and automated measures. Down-sampling and scaling factors were applied to reduce data size and speed up the algorithm. Consequently, Spatial and low contrast resolution were reduced, which may have impacted upon observer variability, making it difficult to differentiate between tissue borders (8,31). This may have impaired the ability of the algorithm to accurately identify and track specific anatomical landmarks.

Study limitations

Similar to other comparable studies, the present study used a small sample of CT scans. This reflects the nature of the patient population being evaluated and the practice of our institute whereby retrospective ECG-gated cardiac CT scans are only performed for specific clinical indications. Despite this, our study demonstrates comparable results to previous research. It remains possible that our findings may not be reflective of larger patient cohorts. This may be owing to the use of cardiac CT scans with retrospectively ECG gated reconstruction and multiple phases available for analysis. This enabled large comparisons (approximately 3000 measurements across 340 phases) to be made not only between patients, but between the manual and automated methods. Furthermore, the performance of the automated algorithm when compared to manual values was entirely dependent on the initial observer measurements made in both methods at phase 0%. Accounting for intra-observer variability it is unlikely that the automated algorithm would have demonstrated perfect or even strong agreement with manual values given the initial differences at phase 0%. Interobserver variability for the manual measurements was unavailable for the current study owing to the requirement for specialised assessment of mitral valve evaluation for TMVR suitability.

Conclusion

In patients with dilated cardiomyopathy, mitral annulus dimensions vary little during the cardiac cycle. D-shaped mitral valve dimensions reveal significant variability between patients with anterior to posterior horn expansion seemingly contributing to overall increased annular dimensions. Owing to the interpatient variability in mitral valve annulus measurements our study indicates the necessity for a tailored, individual approach to TMVR device design and development. In this regard, automated mitral valve evaluation techniques may provide a reliable substitute for lengthy manual CT dataset evaluation.

References

1. Testa L, Latib A, Montone RA, Bedogni F. Transcatheter mitral valve regurgitation treatment: State of the art and a glimpse to the future. The Journal of Thoracic and Cardiovascular Surgery [Internet]. 2016.

2. Makkar RR, Fontana GP, Jilaihawi H, Kapadia S, Pichard AD, Douglas PS, et al. Transcatheter Aortic-Valve Replacement for Inoperable Severe Aortic Stenosis. New England Journal of Medicine. 2012 May 3;366(18):1696–704.

3. Blanke P, Naoum C, Webb J, Dvir D, Hahn RT, Grayburn P, et al. Multimodality Imaging in the Context of Transcatheter Mitral Valve Replacement: Establishing Consensus Among Modalities and Disciplines. JACC: Cardiovascular Imaging. 2015 Oct;8(10):1191–208.

4. Cheung A, Webb J, Verheye S, Moss R, Boone R, Leipsic J, et al. Short-Term Results of Transapical Transcatheter Mitral Valve Implantation for Mitral Regurgitation. Journal of the American College of Cardiology. 2014 Oct 28;64(17):1814–9.

5. Blanke P, Dvir D, Cheung A, Ye J, Levine RA, Precious B, et al. A simplified D-shaped model of the mitral annulus to facilitate CT-based sizing before transcatheter mitral valve implantation. Journal of Cardiovascular Computed Tomography. 2014 Nov;8(6):459–67.

6. Natarajan N, Patel P, Bartel T, Kapadia S, Navia J, Stewart W, et al. Peri-procedural imaging for transcatheter mitral valve replacement. Cardiovasc Diagn Ther. 2016 Apr;6(2):144–59.

7. Levack MM, Jassar AS, Shang EK, Vergnat M, Woo YJ, Acker MA, et al. Three-Dimensional Echocardiographic Analysis of Mitral Annular Dynamics. Circulation. 2012 Sep 11;126(11 suppl 1):S183–8.

8. Leipsic J, Blanke P. Image quality is key in CT for transcatheter aortic valve replacement. Journal of Cardiovascular Computed Tomography. 2016 Sep;10(5):375–6.

9. Achenbach S, Delgado V, Hausleiter J, Schoenhagen P, Min JK, Leipsic JA. SCCT expert consensus document on computed tomography imaging before transcatheter aortic valve implantation (TAVI)/transcatheter aortic valve replacement (TAVR). J Cardiovasc Comput Tomogr. 2012 Dec;6(6):366–80.

10. Blanke P, Dvir D, Cheung A, Levine RA, Thompson C, Webb JG, et al. Mitral Annular Evaluation With CT in the Context of Transcatheter Mitral Valve Replacement. JACC: Cardiovascular Imaging. 2015 May;8(5):612–5.

11. Naoum C, Leipsic J, Cheung A, Ye J, Bilbey N, Mak G, et al. Mitral Annular Dimensions and Geometry in Patients With Functional Mitral Regurgitation and Mitral Valve Prolapse: Implications for Transcatheter Mitral Valve Implantation. JACC: Cardiovascular Imaging. 2016 Mar;9(3):269–80.

12. Di Mauro M, Gallina S, D'Amico MA, Izzicupo P, Lanuti P, Bascelli A, et al. Functional mitral regurgitation: From normal to pathological anatomy of mitral valve. International Journal of Cardiology. 2013 Mar 10;163(3):242–8.

13. Thériault-Lauzier PP, Dorfmeister M, Mylotte D, Andalib A, Spaziano M, Blanke P, et al. Quantitative multi-slice computed tomography assessment of the mitral valvular complex for transcatheter mitral valve interventions part 2: geometrical measurements in patients with functional mitral regurgitation. EuroIntervention. 2015 Nov 23;11(7).

14. Beaudoin J, Thai W-E, Wai B, Handschumacher MD, Levine RA, Truong QA. Assessment of Mitral Valve Adaptation with Gated Cardiac Computed Tomography: Validation with Three-Dimensional Echocardiography and Mechanistic Insight to Functional Mitral Regurgitation. Circ Cardiovasc Imaging [Internet]. 2013 Sep.

15. Alkadhi H, Desbiolles L, Stolzmann P, Leschka S, Scheffel H, Plass A, et al. Mitral Annular Shape, Size, and Motion in Normals and in Patients With Cardiomyopathy: Evaluation With Computed Tomography. Investigative Radiology. 2009 Apr;44(4):218–25.

16. Murphy DT, Blanke P, Alaamri S, Naoum C, Rubinshtein R, Pache G, et al. Dynamism of the aortic annulus: Effect of diastolic versus systolic CT annular measurements on device selection in transcatheter aortic valve replacement (TAVR). Journal of Cardiovascular Computed Tomography. 2016 Jan;10(1):37–43.

17. Blanke P, Spira EM, Ionasec R, Meinel FG, Ebersberger U, Scheuering M, et al. Semiautomated Quantification of Aortic Annulus Dimensions on Cardiac CT for TAVR. JACC: Cardiovascular Imaging. 2014 Mar;7(3):320–2.

18. Wu L, Germans T, Güçlü A, Heymans MW, Allaart CP, van Rossum AC. Feature tracking compared with tissue tagging measurements of segmental strain by cardiovascular magnetic resonance. J Cardiovasc Magn Reson. 2014 Jan 22;16(1):10.

19. Evin M, Redheuil A, Soulat G, Perdrix L, Ashrafpoor G, Giron A, et al. Left atrial aging: a cardiac magnetic resonance feature-tracking study. American Journal of Physiology - Heart and Circulatory Physiology. 2016 Mar 1;310(5):H542–9.

20. Blanke P, Naoum C, Dvir D, Bapat V, Ong K, Muller D, et al. Predicting LVOT Obstruction in Transcatheter Mitral Valve Implantation: Concept of the Neo-LVOT. JACC: Cardiovascular Imaging [Internet]. 2016.

21. Thériault-Lauzier P, Mylotte D, Dorfmeister M, Spaziano M, Andalib A, Mamane S, et al. Quantitative multi-slice computed tomography assessment of the mitral valvular complex for transcatheter mitral valve interventions part 1: systematic measurement methodology and inter-observer variability. EuroIntervention. 2015 Nov 23;11(7).

22. Rausch MK, Bothe W, Kvitting J-PE, Swanson JC, Ingels NB, Miller DC, et al. Characterization of mitral valve annular dynamics in the beating heart. Ann Biomed Eng. 2011 Jun;39(6):1690–702.

23. McBride JB, McBride G, McBride G, McBride GB, McBride GB, McBride G, et al. A proposal for strength-of-agreement criteria for Lin's Concordance Correlation Coefficient. 2005 Jan 1.

24. Mas PT, Rodríguez-Palomares JF, Antunes MJ. Secondary tricuspid valve regurgitation: a forgotten entity. Heart. 2015 Nov 15;101(22):1840–8.

25. Nishimura RA, Vahanian A, Eleid MF, Mack MJ. Mitral valve disease—current management and future challenges. The Lancet. 2016 Mar;387(10025):1324–34.

26. Blanke P, Park JK, Grayburn P, Naoum C, Ong K, Kohli K, et al. Left ventricular access point determination for a coaxial approach to the mitral annular landing zone in transcatheter mitral valve replacement. Journal of Cardiovascular Computed Tomography [Internet]. 2017 Apr.

27. Witkowski TG, Thomas JD, Delgado V, van Rijnsoever E, Ng ACT, Hoke U, et al. Changes in left ventricular function after mitral valve repair for severe organic mitral regurgitation. Ann Thorac Surg. 2012 Mar;93(3):754–60.

28. Saisho H, Arinaga K, Kikusaki S, Hirata Y, Wada K, Kakuma T, et al. Long term results and predictors of left ventricular function recovery after aortic valve replacement for chronic aortic regurgitation. Ann Thorac Cardiovasc Surg. 2015;21(4):388–95.

29. Blanke P, Pibarot P, Hahn R, Weissman N, Kodali S, Thourani V, et al. Computed Tomography–Based Oversizing Degrees and Incidence of Paravalvular Regurgitation of a New Generation Transcatheter Heart Valve. JACC: Cardiovascular Interventions. 2017 Apr;10(8):810–20.

30. Taylor RJ, Moody WE, Umar F, Edwards NC, Taylor TJ, Stegemann B, et al. Myocardial strain measurement with feature-tracking cardiovascular magnetic resonance: normal values. European Heart Journal – Cardiovascular Imaging. 2015 Aug;16(8):871–81.

31. Soon J, Sulaiman N, Park JK, Kueh S-H (Anthony), Naoum C, Murphy D, et al. The effect of a whole heart motion-correction algorithm on CT image quality and measurement reproducibility in Pre-TAVR aortic annulus evaluation. Journal of Cardiovascular Computed Tomography. 2016 Sep;10(5):386–90.

Figure legends

Figure 1

The saddle shaped mitral valve annulus.

Figure 2

Cardiac CT scan: illustration of the manual mitral valve measurements taken in the short axis (A), 2-chamber (B) and 4-chamber (C) views).

Figure 3

Changes in mitral valve annulus measurements throughout the cardiac cycle.

Figure 4

Correlation scatter plots demonstrating agreement between manual and automated assessment of the MV annulus across all phases.

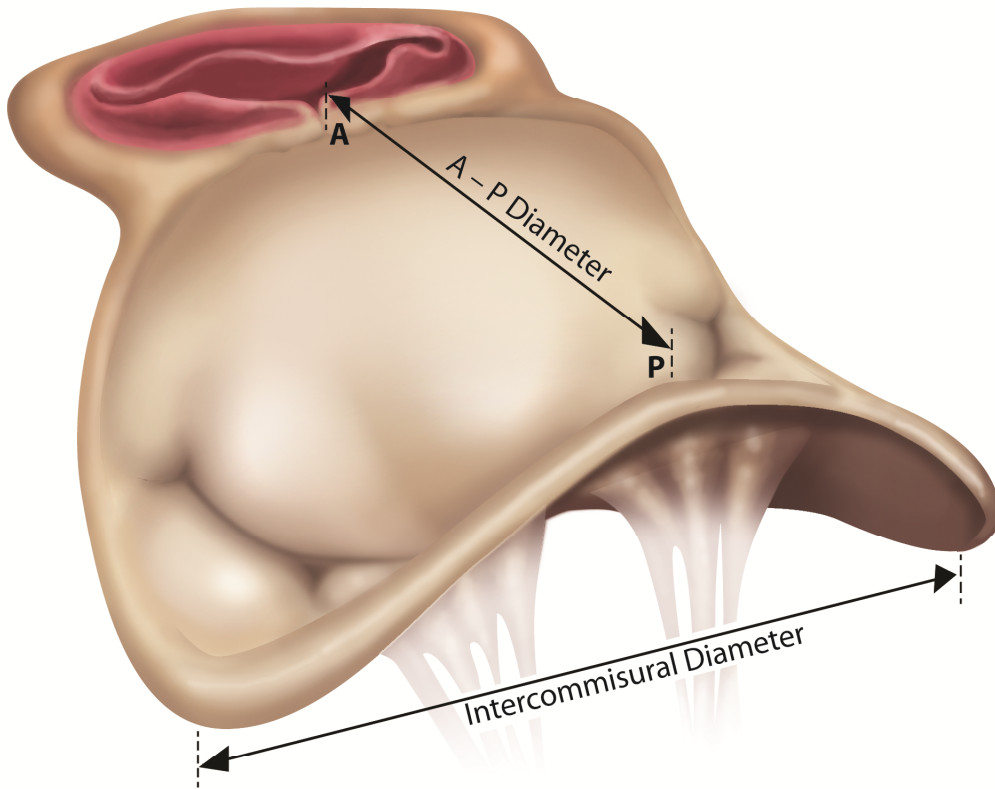| Table 1 MV Assessment and Measurements	
Short Axis	
Trigone to Trigone diameter (TT)	The line connecting medial and lateral fibrous trigones at the aorto-mitral continuity.
Posterior Perimeter (PP)	The posterior perimeter of the mitral annulus was traced originating at the medial trigone around to the lateral trigone.
Mitral Annulus Area (MA_{area})	Mitral annulus area was calculated using the D-shaped model, tracing the posterior perimeter of the annulus and truncating the anterior horn across a straight line.
Intercommissural Diameter (IC)	Intercommissural diameter was taken parallel to the truncated trigone to trigone line, transecting the centre of the mitral annulus.
Anterior to Posterior Diameter (AP)	Bisecting the left ventricular outflow tract and perpendicular to the IC diameter, the diameter of the posterior peak was measured to the anterior TT line.
4 Chamber view	
MA geometric centre to Endocardial border of LV apex (LV_{endo})	With both 2 chamber and 4 chamber views bisecting the left ventricular apex, the distance taken from the mitral valve geometric centre to the endocardial border was measured.
MA geometric centre to Epicardial border of LV	With both 2 chamber and 4 chamber views bisecting the left ventricular apex, the distance taken from the mitral valve

apex (LV$_{epi}$)	geometric centre to the epicardial border was measured.
MA geometric centre to head of the Anterolateral Papillary Muscle (PM-al)	The mitral valve geometric centre was extended to the most superior aspect of the anterolateral papillary muscle head.
MA geometric centre to head of the Posteromedial Papillary Muscle (PM-pm)	The mitral valve geometric centre was extended to the most superior aspect of the posteromedial papillary muscle head.
2 chamber view	
MA geometric centre to posterior wall of the left atrium (LA-lad)	The long axis diameter of the left atrium was measured from the geometric centre of the annulus to the inside edge of the left atrial posterior wall.

Table 2 Baseline Characteristics	
Clinical	
Age, years	68 ± 15
Female, n	4
QRS, ms	175 ± 22
NYHA Class, n	
II	1
II/III	3
III/IV	11
LV EF, %	36 ± 12
LA area, cm^2	26.3 ± 5.5

Table 3 Mean dimensions for systole and diastole across all measurements

	Systole (30%)		Diastole (60%)			
	Mean ± SD	Interquartile (Q1, Q3)	Mean ± SD	Interquartile (Q1, Q3)	% change	*p* (95% CI)
Short Axis						
Mitral Annulus Area (cm^2)	11.6 ± 1.6	10.6, 13.4	12.2 ± 1.9	11.0, 13.4	5.5%	*p* = 0.045 (-128.9, -1.7)
Posterior Perimeter (mm)	98.5 ± 6.8	92.3, 107.0	100.5 ± 8.2	94.7, 104.7	2.0%	*p* = 0.16 (-4.85, 0.89)
Trigone to trigone Diameter (mm)	25.0 ± 2.8	23.2, 26.9	25.9 ± 2.0	24.6, 27.3	3.3%	*p* = 0.14 (-1.975, 0.295)
Intercommissural Diameter (mm)	41.3 ± 2.9	39.6, 43.5	41.6 ± 3.3	38.6, 43.0	0.8%	*p* = 0.58 (-1.601, 0.934)
Anterior to Posterior Diameter (mm)	32.8 ± 3.1	30.4, 34.7	34.6 ± 3.4	32.0, 36.2	5.3%	*p* = 0.005 (-2.957, -0.643)
4 Chamber						
MV centre to LV apex - Endocardium (mm)	90.9 ± 10.7	83.8, 96.3	90.5 ± 9.2	81.8, 94.9	0.5%	*p* = 0.71 (-2.16, 3.08)
MV centre to LV apex - Epicardium (mm)	96.4 ± 10.9	88.7, 101.4	95.9 ± 9.6	88.4, 100.2	0.5%	*p* = 0.30 (-5.13, 15.65)
MV centre to AL papillary muscle (mm)	25.6 ± 4.5	21.9, 28.7	25.2 ± 4.3	21.3, 28.9	1.5%	*p* = 0.74 (-2.01, 2.76)
MV centre to PM papillary muscle (mm)	29.2 ± 3.9	26.1, 32.3	30.3 ± 4.5	25.5, 34.5	3.7%	*p* = 0.32 (-3.33, 1.16)
2 Chamber						
MV centre to LA superior wall diameter (mm)	58.5 ± 9.1	50.9, 64.2	57.7 ± 9.8	50.1, 65.1	1.4%	*p* = 0.48 (-1.62, 3.30)

Table 4 Paired sample T-tests at phase 0% and Lin's Concordance correlation coefficient to measure agreement between manual and automatic values

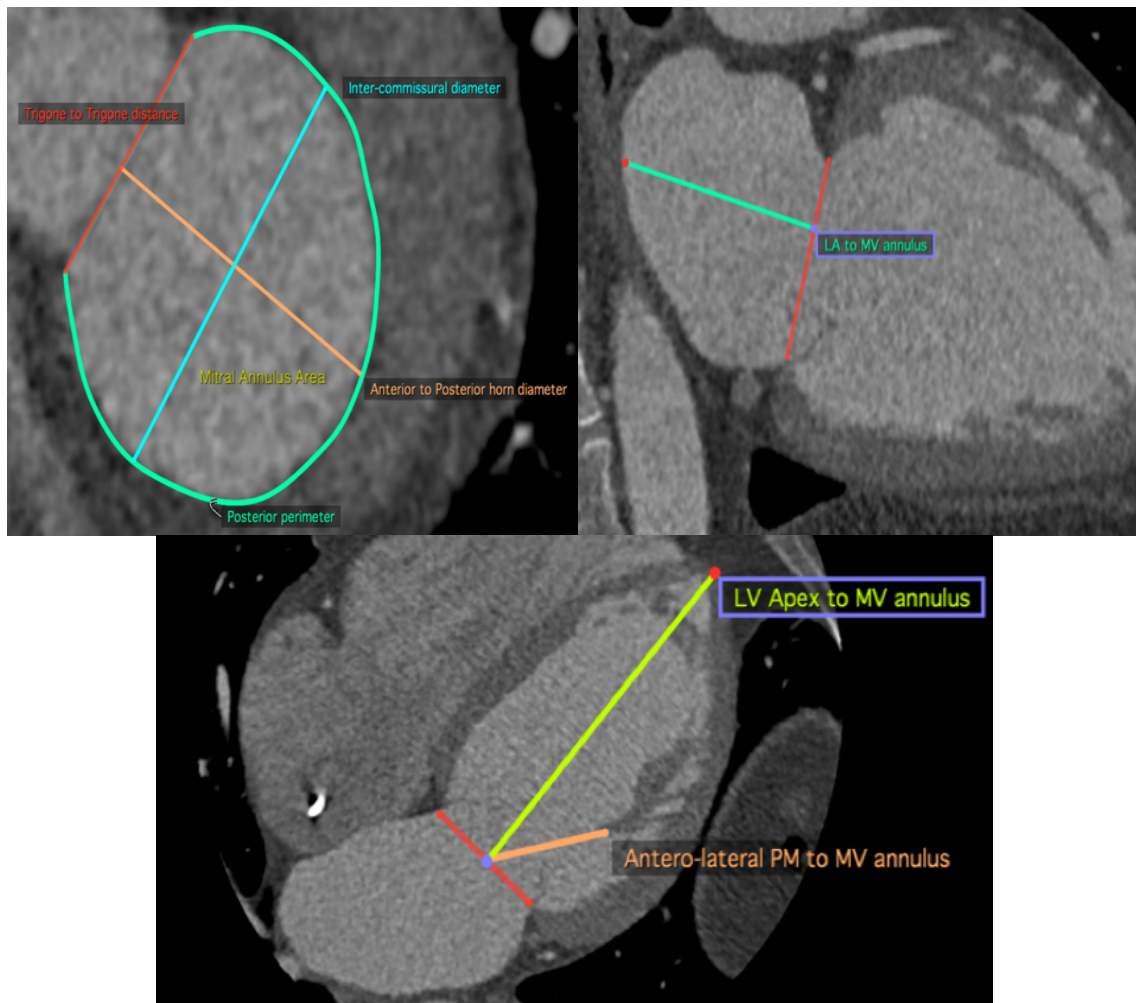| Measure	T-Test at 0%, *p*, (95% CI)	Lin's CCC - ρ_c
Trigone to Trigone Diameter	*p* = 0.001 (1.335, 3.585)	0.27
Posterior perimeter	*p* = 0.99 (-2.65, 2.61)	0.76
Mitral annulus area	*p* = 0.15 (-0.133, 0.797)	0.75
Intercommissure diameter	*p* = 0.16 (-0.251, 1.424)	0.73
Posterior to anterior horn diameter	*p* = 0.13 (-0.391, 2.634)	0.62
Mitral annulus to LV apex (endocardium) distance	*p* = 0.04 (-5.01, -0.15)	0.90
Mitral annulus to LV apex (epicardium) distance	*p* = 0.73 (-3.53, 2.52)	0.86
Mitral annulus to antero-lateral papillary muscle head distance	*p* = 0.001(2.254, 6.026)	0.47
Mitral annulus to postero-medial papillary muscle head distance	*p* = 0.008 (0.707, 4.013)	0.68
Mitral annulus to left atrial superior wall	*p* = 0.63 (-2.97, 1.85)	0.84

Figure 2 (Clockwise – A, B, C).

Figure 3

Line Graph illustrating mean change in anterior to posterior horn diameter across the full cardiac cycle (0%-90%).

Line Graph illustrating change in inter-commissure distance across the full cardiac cycle (0%-90%).

Line Graph illustrating change in mitral annulus area across the full cardiac cycle (0%-90%).

Line Graph illustrating change in Posterior annulus perimeter across the full cardiac cycle (0%-90%).

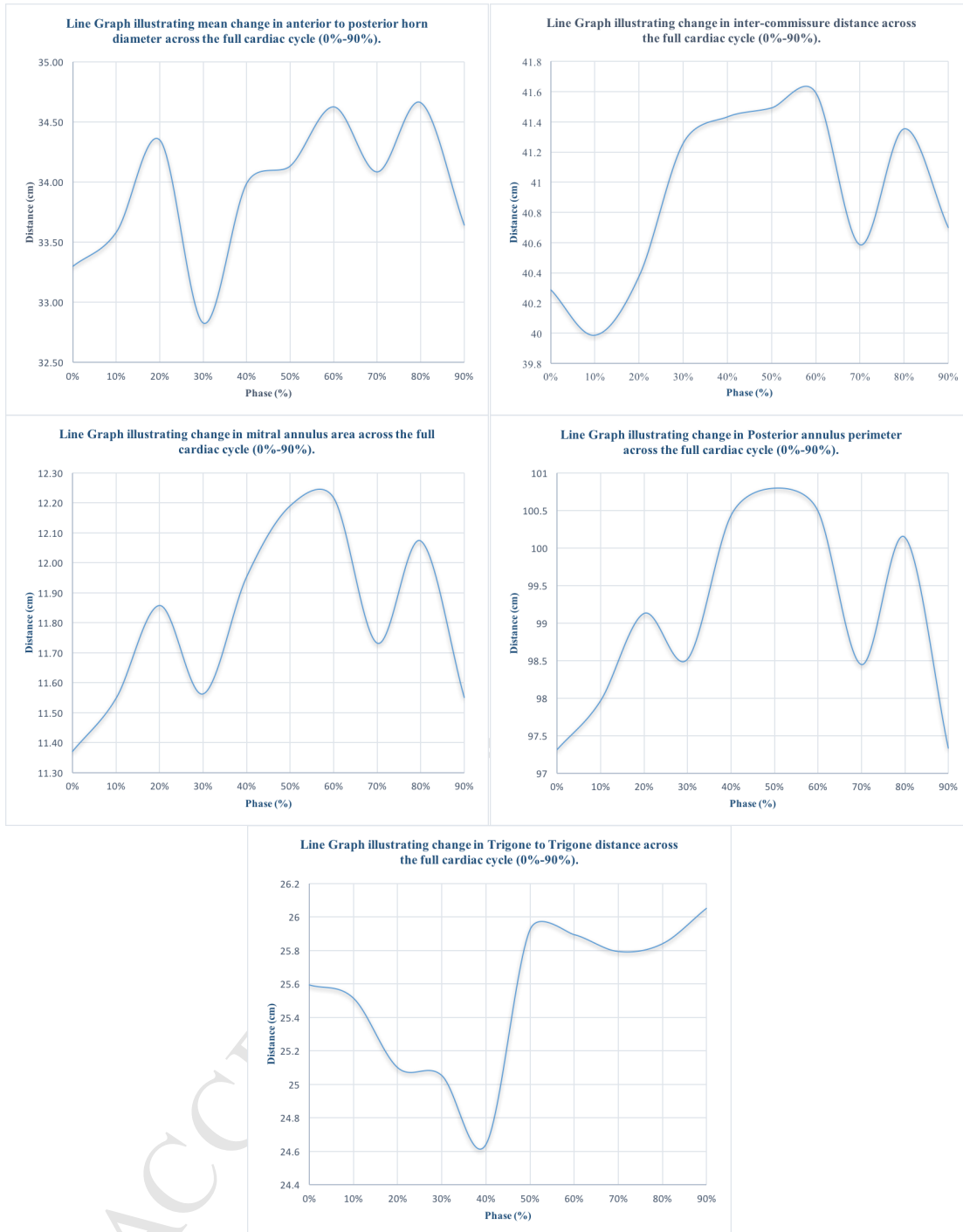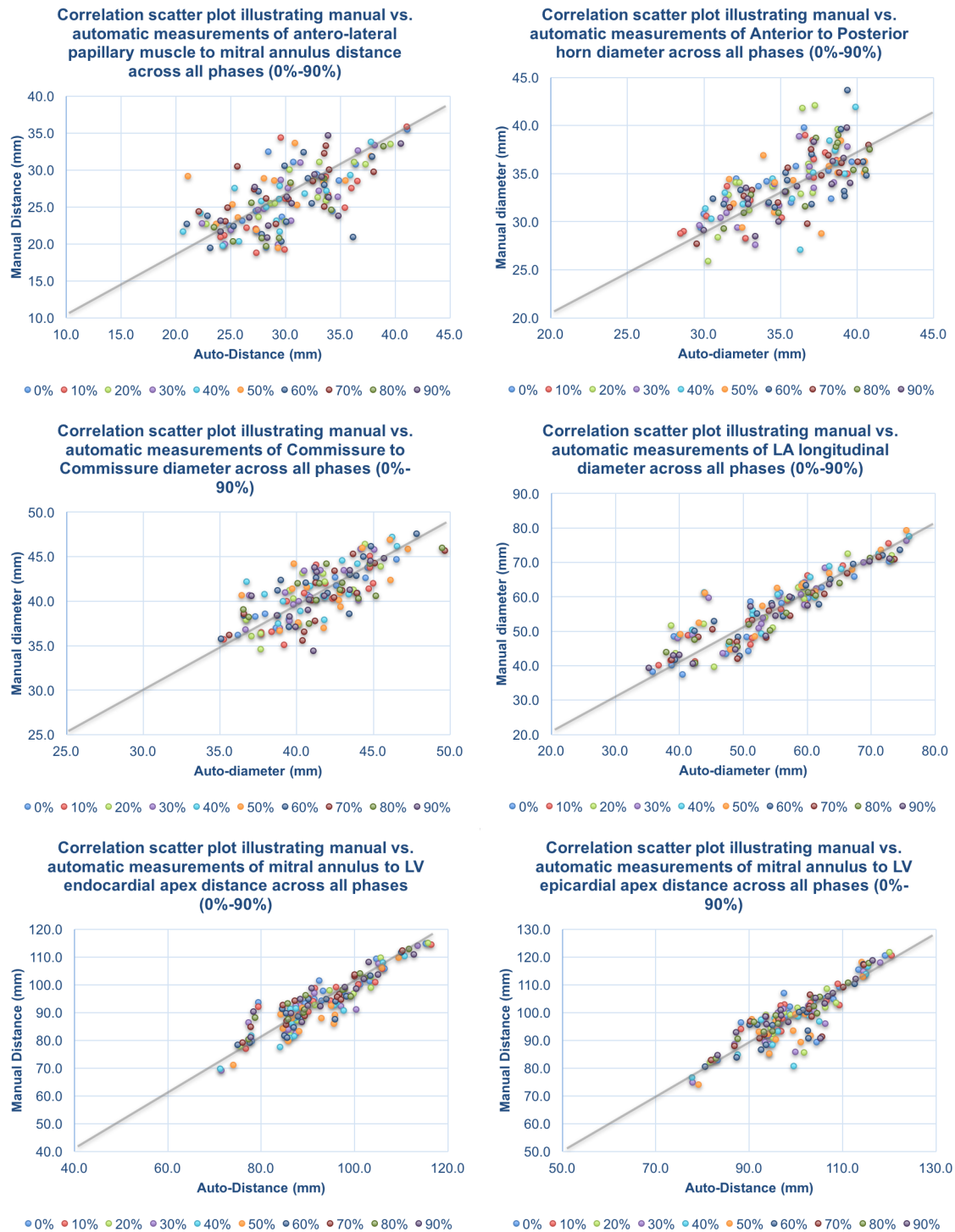Line Graph illustrating change in Trigone to Trigone distance across the full cardiac cycle (0%-90%).

Figure 4

Correlation scatter plot illustrating manual vs. automatic measurements of antero-lateral papillary muscle to mitral annulus distance across all phases (0%-90%)

Correlation scatter plot illustrating manual vs. automatic measurements of Anterior to Posterior horn diameter across all phases (0%-90%)

Correlation scatter plot illustrating manual vs. automatic measurements of Commissure to Commissure diameter across all phases (0%-90%)

Correlation scatter plot illustrating manual vs. automatic measurements of LA longitudinal diameter across all phases (0%-90%)

Correlation scatter plot illustrating manual vs. automatic measurements of mitral annulus to LV endocardial apex distance across all phases (0%-90%)

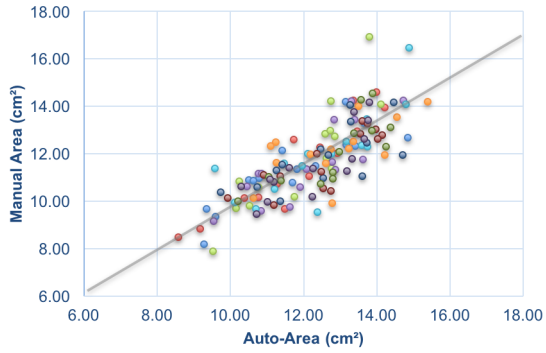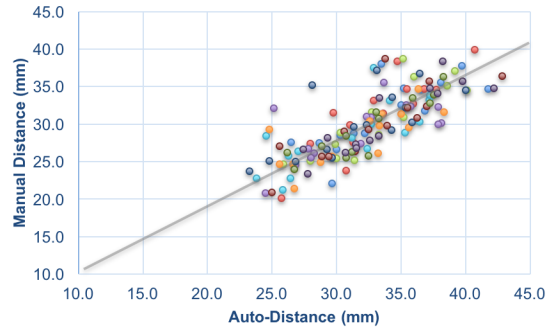Correlation scatter plot illustrating manual vs. automatic measurements of mitral annulus to LV epicardial apex distance across all phases (0%-90%)

Correlation scatter plot illustrating manual vs. automatic measurements of Mitral Annulus Area across all phases (0%-90%)
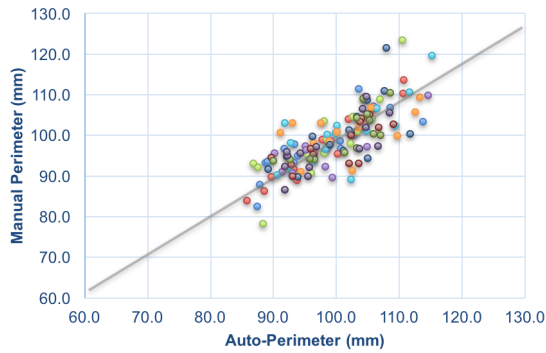

Correlation scatter plot illustrating manual vs. automatic measurements of postero-medial papillary muscle to mitral annulus distance across all phases (0%-90%)
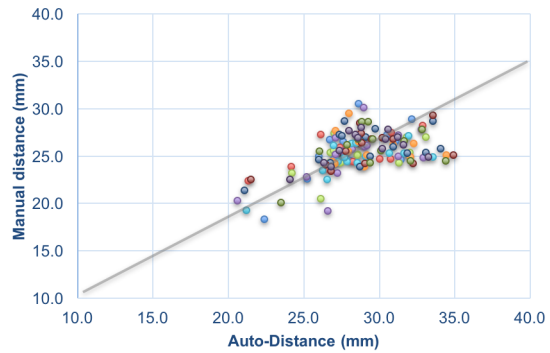

Correlation scatter plot illustrating manual vs. automatic measurements of the posterior annulus perimeter across all phases (0%-90%)

Correlation scatter plot illustrating manual vs. automatic measurements of trigone to trigone distance across all phases (0%-90%)